# Supporting Information

## Synergistic co-doping induced high catalytic activities of La/Fe doped $Co_3O_4$ towards oxygen reduction/evolution reactions for Zn-air batteries

Zhongyuan Xia,[a] Binglu Deng,[b] Yongjie Wang,[c] Zhongqing Jiang [d] and Zhong-Jie Jiang*[a]

[a] *Guangzhou Key Laboratory for Surface Chemistry of Energy Materials, Guangdong Engineering and Technology Research Center for Surface Chemistry of Energy Materials, College of Environment and Energy, South China University of Technology, Guangzhou 510006, P. R. China. E-mail: eszjiang@scut.edu.cn and zhongjiejiang1978@hotmail.com.*

[b] *School of Materials Science and Hydrogen Energy, Foshan University, Foshan 52800, P. R. China.*

[c] *School of Science, Harbin Institute of Technology, Shenzhen 518055, P. R. China.*

[d] *Key Laboratory of Optical Field Manipulation of Zhejiang Province, Department of Physics, Zhejiang Sci-Tech University, Hangzhou 310018, P. R. China.*

**This file includes:**

**Experimental Section**

**DFT calculations**

**Figures. S1 to S11**

**Tables S1**

## Experimental Section

### Chemicals

Concentrated sulfuric acid ($H_2SO_4$, 95~98.0%) and concentrated nitric acid ($HNO_3$, 65.0~68.0%) were obtained from Guangzhou Chemical Reagent Co, Ltd. Cobalt acetate ($Co(Ac)_2$, 99.0%), ammonium hydroxide ($NH_4OH$, 25%), ethyl alcohol ($C_2H_5OH$, 99.7%), N,N-dimethylformamide (DMF, AR), potassium hydroxide (KOH, 85%) and dopamine hydrochloride were purchased from Da Mao Chemical Company. Nafion (5 wt% solution) were obtained from DuPont. The Pt/C with 20 wt% Pt obtained from the Johnson Matthey Corp. was used for the comparison. All the reagents were utilized as provided. Deionized (DI) water with a resistance of 18.2 MΩ $cm^{-1}$ was used in all the experiments.

### Material synthesis

#### Synthesis of $La_{0.23}Fe_{0.15}$-$Co_3O_4$/NCNTs

1.0 mL of the $Co(Ac)_2$ ethanol solution (0.1 mol $L^{-1}$), 2.5 mL of the $LaCl_3$ ethanol solution (0.01 mol $L^{-1}$), 2.0 mL of the $Fe(Ac)_3$ ethanol solution (0.01 mol $L^{-1}$) and 15.0 mg of the aminated carbon nanotubes (NCNTs, synthesized by a reported method[1]) were first mixed together. 25.0 mL of DMF and 19.5 mL of ethanol were then added to give 50.0 mL of a homogeneous solution with $V_{DMF}$:$V_{EtOH}$ = 1:1 under ultrasonication. The mixture was refluxed at 80 °C, followed by the dropwise addition of 2.0 mL $NH_4OH$ (25%). After 3.0 h of stirring at 80 °C, the obtained solution was transferred to a 100 mL Teflon-lined autoclave and solvothermally heated at 150 °C for 3.0 h. After cooling, the precipitate was collected through centrifugation and successfully washed with water and ethanol for > 3 times. The ICP-OES analysis showed that the molar ratio of La:Fe:Co was 0.23:0.15:1.00, suggesting the formation of the $La_{0.23}Fe_{0.15}$-$Co_3O_4$/NCNTs. For comparison, the La-$Co_3O_4$/NCNTs and Fe-$Co_3O_4$/NCNTs with various doping levels were fabricated using the same procedure used for the synthesis of the $La_{0.23}Fe_{0.15}$-$Co_3O_4$/NCNTs, while in the absence of $FeCl_3$ and $LaCl_3$, respectively. Additionally, the LaFe-$Co_3O_4$/NCNTs with a fixed La doping level (La:Co =

0.23:1.00) and various Fe doping levels were synthesized by the same method through controlling the dosage of $FeCl_3$.

**Synthesis of C@$La_{0.23}Fe_{0.15}$-$Co_3O_4$/NCNTs**

10.0 mg of the $La_{0.23}Fe_{0.15}$-$Co_3O_4$/NCNTs synthesized above were dispersed in 30.0 mL of Tris-buffer (pH ~ 8.5) by ultrasonication for 0.5 h to form a suspension. 20.0 mg of dopamine hydrochloride was subsequently added under stirring. The reaction was last for 6.0 h under the continuous stirring at room temperature. The precipitates were collected by centrifugation, washed 3 times with DI water, and dried at 60 °C for 12.0 h. The resulting sample was heated in a quartz tube at 300°C for 2.0 h under the $N_2$ atmosphere. This led to the formation of the C@$La_{0.23}Fe_{0.15}$-$Co_3O_4$/NCNTs.

**Material characterization**

An X-ray diffractometer (XRD, Bruker D8 Advance diffractometer, Germany) with Cu Kα radiation (λ = 1.5406 Å) was employed to identify the sample crystal structures. The TEM images were taken on Transmission electron microscopy (TEM, JEOL JEM-2100F, Japan) operated at 200 kV. The energy-dispersive X-ray spectroscopic (EDS) mapping was imaged on a scanning electron microscope (FESEM, Hitachi SU8010, Japan) operated at 15 kV. X-ray photoelectron spectrometer (XPS, Thermo Fisher Nexsa, USA) with Al Kα radiation was applied to analyze the elemental compositions of the samples. Inductively coupled plasma optical emission spectrometry (ICP-OES, Thermo Fisher iCAP 7200 Duo, USA) was used to analyze the content of metal elements in samples.

**Electrochemical measurement**

All the electrochemical tests were performed on an electrochemical workstation (Chenhua, CHI 760E) coupled with a PINE rotating instrument using a standard three-electrode system.

The working electrode was prepared by dropping the catalyst ink on the disk electrode and dried naturally. The mass loading of the catalyst was controlled to be ~ 0.15 mg $cm^{-2}$. The catalyst ink was prepared by dispersing 3.0 mg of the catalyst in 1.0 mL of the isopropanol/water solution with an isopropanol:water volume ratio of 7:3 and 10 μL 5 wt% Nafion solution, followed by ultrasonication for 0.5 h. A carbon rod and the saturated Ag/AgCl were employed as the counter and reference electrodes, respectively. The KOH solution (0.1 M) was used as the electrolyte. All the tests were carried out in the electrolyte saturated with $O_2$. Before the data collection, all the catalysts were activated by the cyclic voltammetry for > 10 sweeps. The potentials reported in this work were calibrated to the reversible hydrogen electrode (RHE) using: $E_{RHE} = E_{(Ag/AgCl)} + 0.059 \times pH + 0.197$.

Linear sweep voltammograms (LSVs) of the ORR were collected at rotation rates from 400 to 2500 rpm at 5 mV $s^{-1}$. The electron transfer number ($n$) involved in the ORR was estimated on the basis of the Koutecky-Levich (K-L) equation:

$$\frac{1}{J} = \frac{1}{J_k} + \frac{1}{B\omega^{1/2}} \tag{S1}$$

$$B = 0.62nFC_0D_0^{2/3}\nu^{-1/6} \tag{S2}$$

Where $J$ and $J_k$ represent the measured and kinetic current densities, respectively; $F$ the Faraday constant (96485 C $mol^{-1}$); $\omega$ the angular velocity (rad $s^{-1}$); $C_0$ the bulk $O_2$ concentration in 0.1 M KOH ($1.2\times10^{-3}$ mol $L^{-1}$); $D_0$ the oxygen diffusion coefficient in a 0.1 M KOH solution ($1.9\times10^{-5}$ $cm^2$ $s^{-1}$); and $\nu$ the electrolyte kinematic viscosity (0.01 $cm^2$ $s^{-1}$). The cyclic voltammograms (CVs) of the ORR were collected at a scan rate of 10 mV $s^{-1}$. The chronoamperometric curves in an $O_2$-saturated 0.1 M KOH solution were recorded to assess the ORR stability.

The rotating ring-disk electrode (RRDE) measurements were conducted in the $O_2$-saturated KOH solution (0.1 M) at 5 mV $s^{-1}$ under 1600 rpm. The Pt ring electrode potential

was set to 1.5 V vs. RHE. The estimation of the electron transfer number (*n*) and the percentage of $HO_2^-$ ($\%HO_2^-$) were performed using:

$$n = 4 \times \frac{I_D}{I_D + I_R / N} \tag{S3}$$

$$\%HO_2^- = 200 \times \frac{I_R / N}{I_D + I_R / N} \tag{S4}$$

where $I_D$ and $I_R$ stand for the disk and ring currents, respectively, and $N$ the current collection coefficient of the Pt ring ($N$ = 0.37).

The LSVs of the OER were recorded under 1600 rpm. The electrochemical impedance spectra (EIS) were recorded at the frequencies ranging from $10^{-2}$ to $10^5$ Hz. All the LSVs of OER reported in this work were iR-corrected. The double layer capacitance ($C_{dl}$) was estimated based on the CVs at different scan rates (2~12 mV $s^{-1}$), tested in the non-Faradic potential range. The chronopotentiometric curves were used to evaluate the stability of the OER.

**Zinc–air battery tests**

The performance of the catalysts was evaluated directly in the home-made rechargeable Zn–air batteries. The air electrode was prepared by casting the catalyst ink on the carbon fiber paper to give a mass loading of 1.0 mg $cm^{-2}$ and dried overnight at 50°C. A polished zinc plate and a mixed solution of KOH (6.0 M) and $Zn(Ac)_2$ (0.2 M) were employed as the anode and the electrolyte, respectively. For comparison, the air electrode loaded with Pt/C and $RuO_2$ with a mass ratio of 1:1 was prepared. All the battery tests were carried out in ambient air flow.

**DFT calculations**

Spin-polarized DFT calculations were conducted using the VASP developed by Kresse et al., in which the generalized gradient approximation Perdew-Burke-Ernzerhof exchange-correlation functional and projector augmented wave (PAW) method was used.[2-4] The DFT+U

method with U−J = 3.3 and 4.0 eV for the respective Co and Fe 3d orbitals was used for the calculations. The convergence criteria for the plane-wave energy cutoff and the relaxation force on each atom were set to $1\times10^{-4}$ eV and 0.02 eV $Å^{-1}$, respectively. The Brillouin zone was sampled with Monkhorst-pack k-point meshes. A vacuum layer of 15 Å was applied along z-direction to avoid imaginary interactions.

The evaluations of the ORR/OER activities of a catalyst were performed by calculating the Gibbs free energy change (ΔG) of each elementary step. Specifically, the elementary reaction steps of the ORR with the four-electron transfer pathway in the alkaline solutions can be expressed as follows:

$$*+O_2+H_2O+e^- \rightarrow *OOH+OH^- \quad \text{(S5)}$$

$$*OOH+e^- \rightarrow *O+OH^- \quad \text{(S6)}$$

$$*O+H_2O+e^- \rightarrow *OH+OH^- \quad \text{(S7)}$$

$$*OH+e^- \rightarrow *+OH^- \quad \text{(S8)}$$

Where * represents the active sites of the catalyst. According to the computational hydrogen electrode model proposed by Nørskov et al.,[5] ΔG of each elementary step can be calculated by the following equation:

$$\Delta G=\Delta E+\Delta ZPE-T\Delta S+\Delta G_U+\Delta G_{pH} \quad \text{(S9)}$$

Where ΔE is the calculated binding energy change of the intermediates, ΔZPE and ΔS are the zero-point and entropy changes of each elementary step. $\Delta G_U$ = -eU, in which U represents the applied electrode potential. $\Delta G_{pH}$ represents the ΔG correlation of the electrolyte pH value: $\Delta G_{pH} = k_B T\ln(10)\times pH$. The OER was assumed to occur through the same elementary steps of the ORR in reverse order.

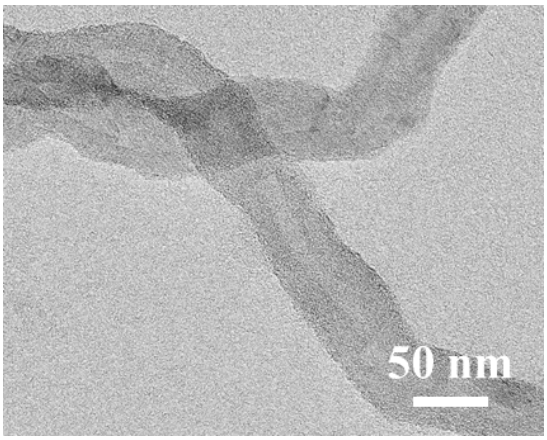


**Figure S1.** Typical TEM image of the NCNTs.

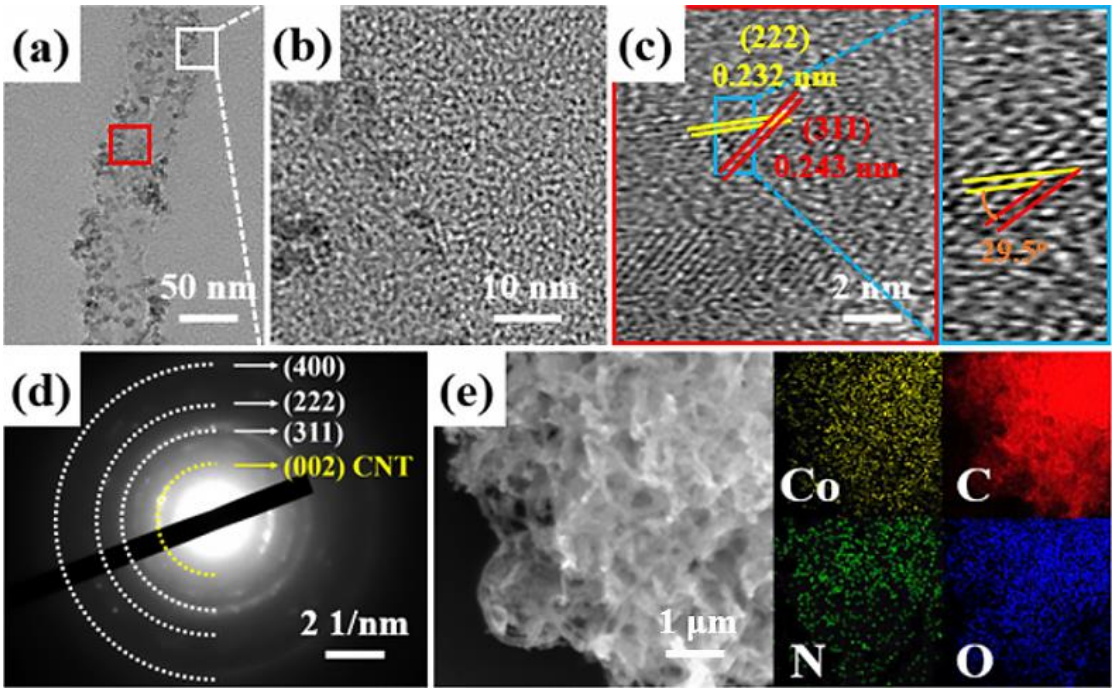


**Figure S2.** (a) TEM, (b) magnified TEM, (c) HRTEM, (d) SAED, (e) elemental mapping images of the $Co_3O_4$/NCNTs.

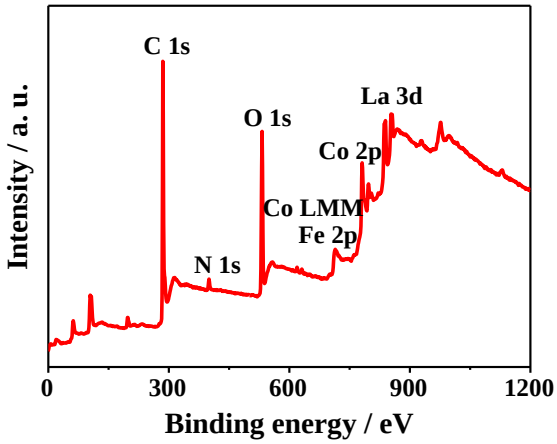


**Figure S3.** Panoramic XPS spectrum of the $La_{0.23}Fe_{0.15}$-$Co_3O_4$/NCNTs.

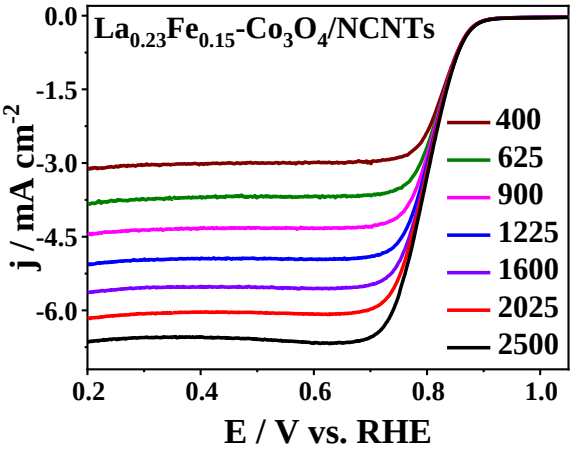


**Figure S4.** LSVs of the $La_{0.23}Fe_{0.15}$-$Co_3O_4$/NCNTs at different rotation rates.

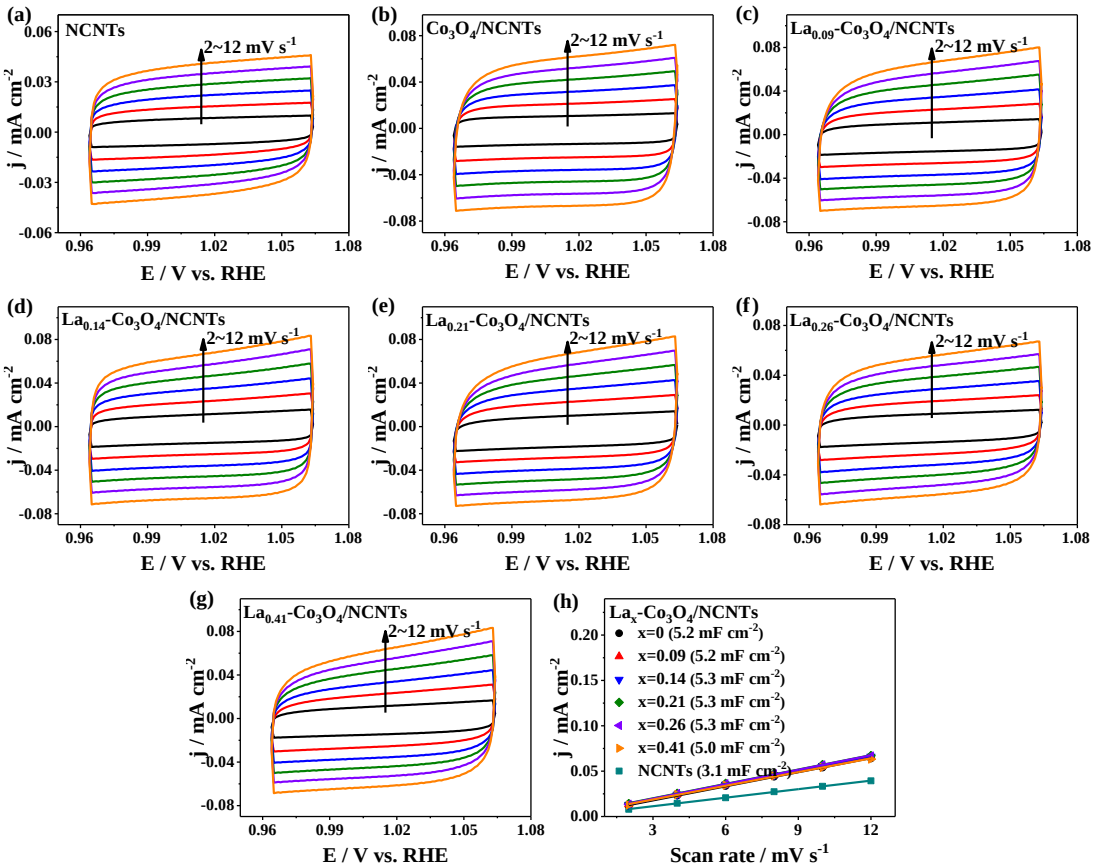


**Figure S5.** CVs of catalysts recorded at different scan rates in the region of 0.964-1.064 V of (a) NCNTs, (b) $Co_3O_4$/NCNTs and (c-g) $La_x$-$Co_3O_4$/NCNTs. (h) $C_{dl}$ plot of the catalysts.

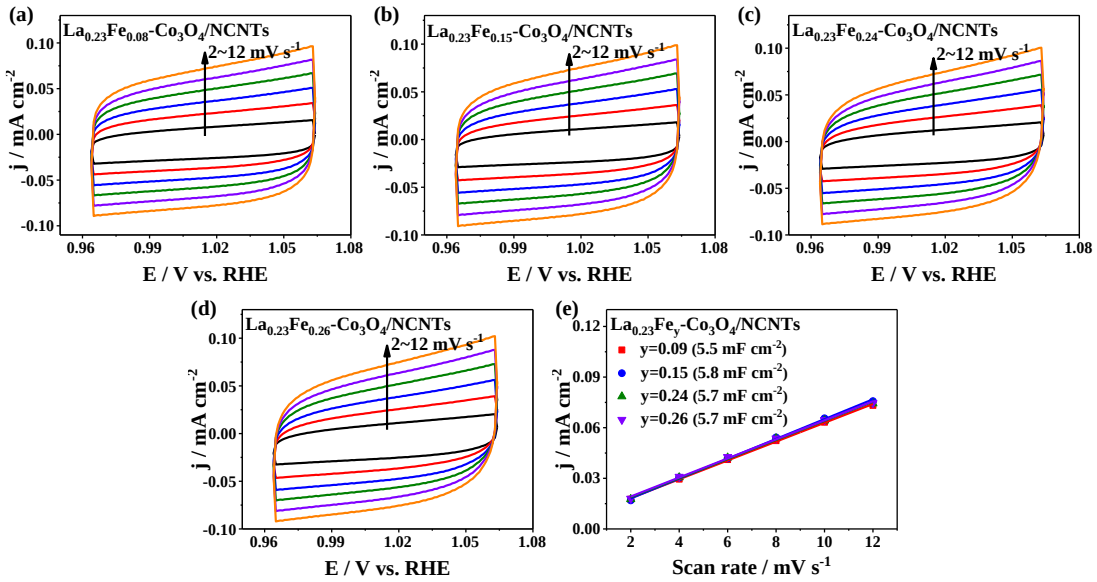


**Figure S6.** CVs of catalysts recorded at different scan rates in the region of 0.964-1.064 V of (a-d) $La_{0.23}Fe_y$-$Co_3O_4$/NCNTs. (e) $C_{dl}$ plot of the catalysts.

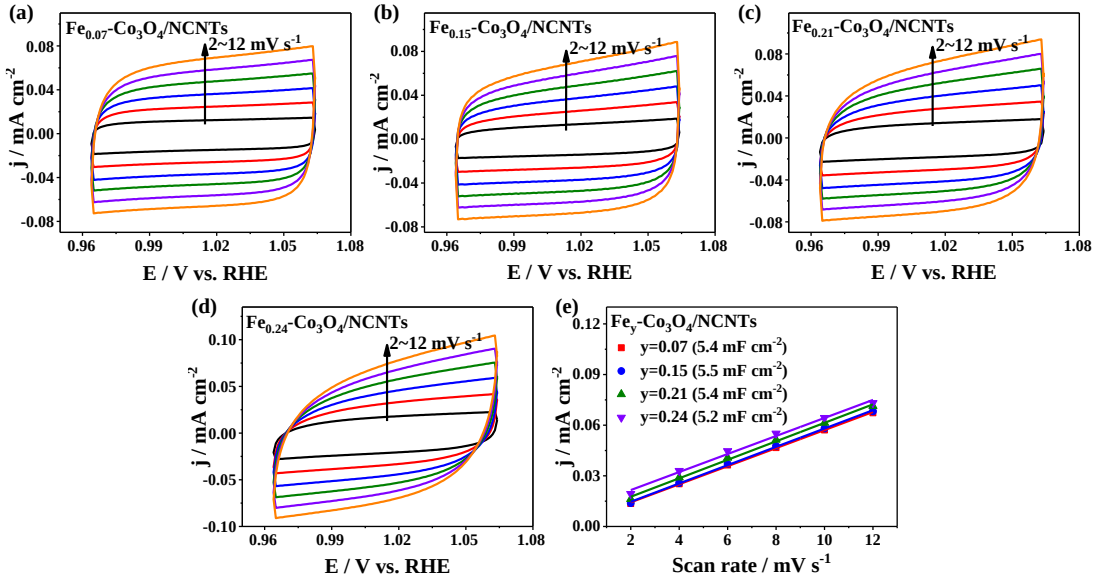


**Figure S7.** CV curves of catalysts recorded at different scan rates in the region of 0.964-1.064 V of (a-d) $Fe_y$-$Co_3O_4$/NCNTs. (e) $C_{dl}$ plot of the catalysts.

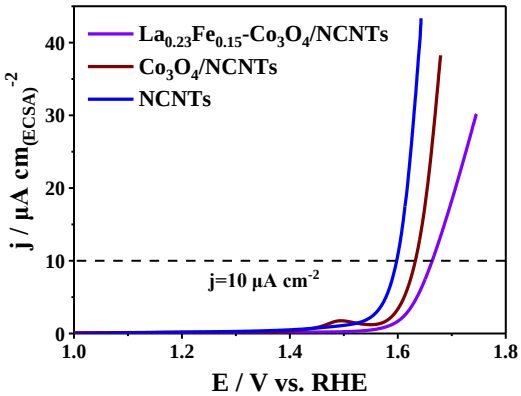


**Figure S8.** Electrochemically surface area (ECSA) normalized OER LSVs for $La_{0.23}Fe_{0.15}$-$Co_3O_4$/NCNTs, $Co_3O_4$/NCNTs and NCNTs.

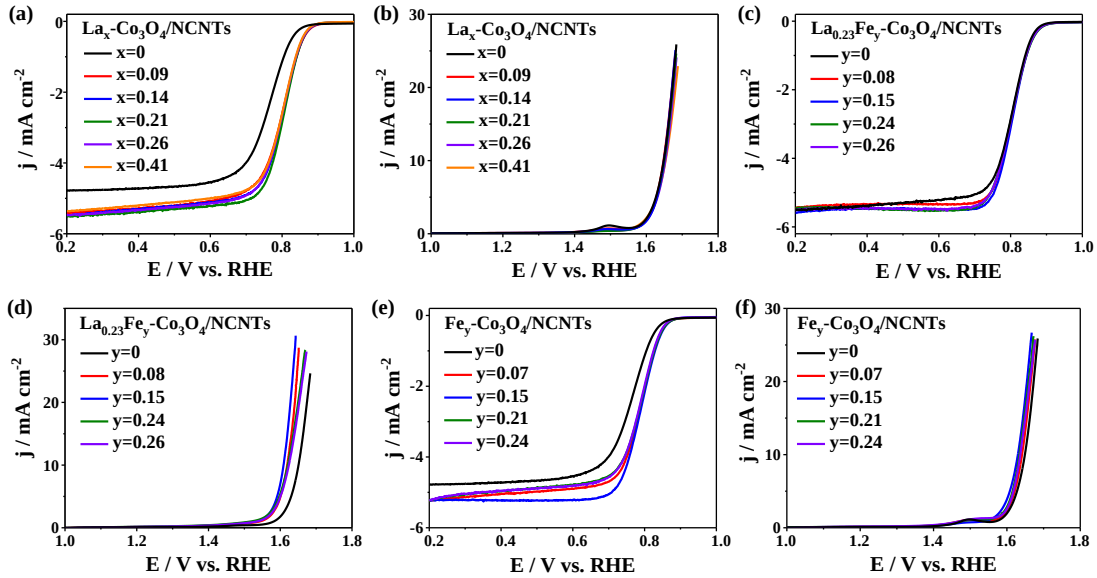


**Figure S9.** (a) ORR LSVs and (b) OER LSVs of La$_x$-Co$_3$O$_4$/NCNTs. (c) ORR LSVs and (d) OER LSVs of La$_{0.23}$Fe$_y$-Co$_3$O$_4$/NCNTs. (e) ORR LSVs and (f) OER LSVs of Fe$_y$-Co$_3$O$_4$/NCNTs.

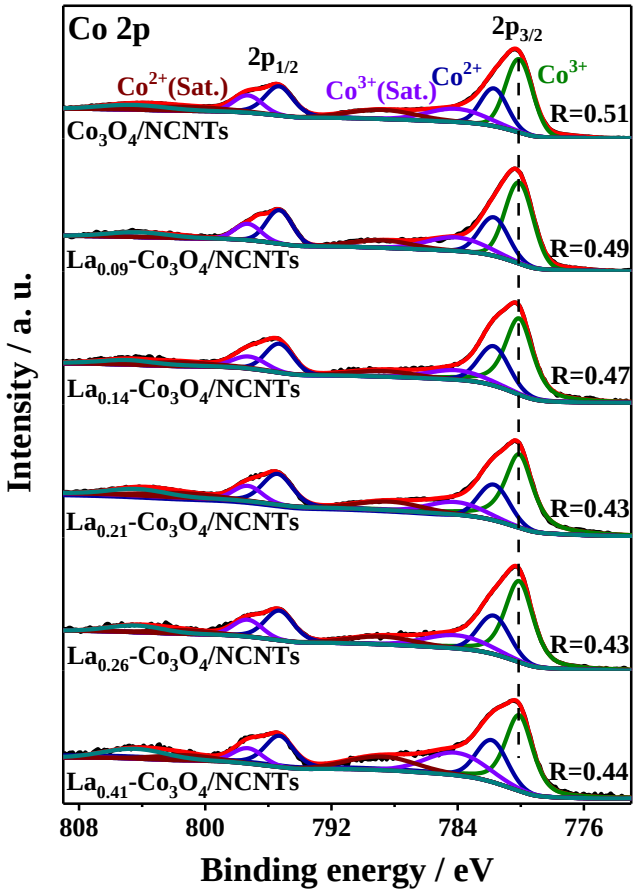


**Figure S10.** Co 2p XPS spectra of the La-Co$_3$O$_4$/NCNTs (R represents the Co$^{2+}$/Co$^{3+}$ ratio).

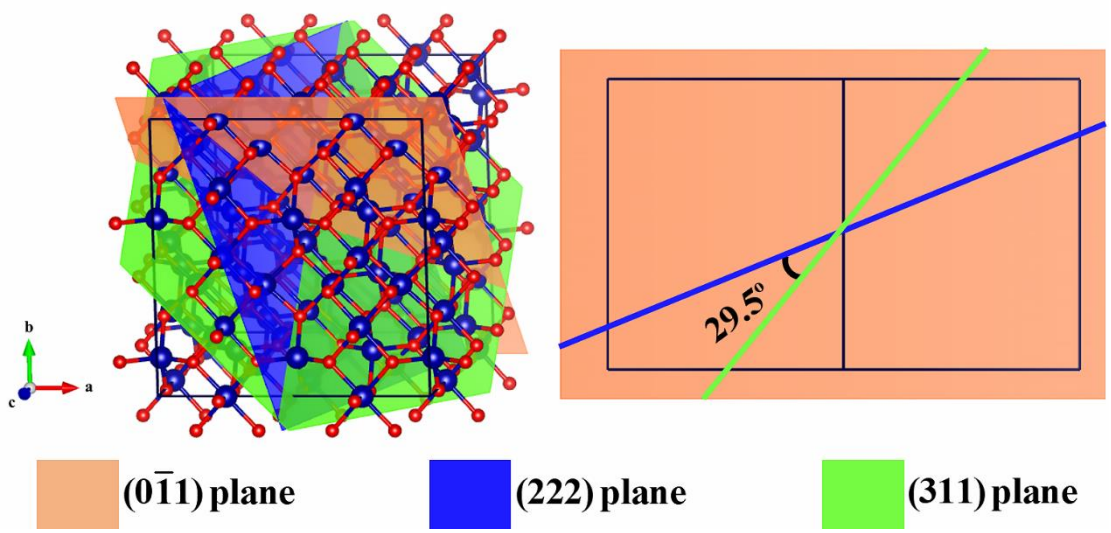


**Figure S11.** Illustration of the exposures of the $(0\bar{1}1)$ plane of $La_{0.23}Fe_{0.15}$-$Co_3O_4$ NPs to catalytic reactions. The $La_{0.23}Fe_{0.15}$-$Co_3O_4$ nanoparticles exhibit the crystalline nature similar to the spinel structure $Co_3O_4$, as demonstrated the XRD patterns in **Figure 2a**. The HRTEM image of the $La_{0.23}Fe_{0.15}$-$Co_3O_4$/NCNTs shows the lattice fringes corresponding to the (311) and (222) planes of the spinel structure $Co_3O_4$. The crystalline plane perpendicular to both the (311) and (222) planes of the spinel structure $Co_3O_4$ will be the exposed facets for the catalytic reactions. As illustrated in figure, the $(0\bar{1}1)$ plane is perpendicular to both the (311) and (222) planes of the spinel structure $Co_3O_4$. It can then be inferred that the $La_{0.23}Fe_{0.15}$-$Co_3O_4$ NPs expose the $(0\bar{1}1)$ plane to catalytic reactions.

**Table S1.** ORR and OER properties of catalysts in this work and recently reported.

| Catalyst | Electrolyte | Loading (mg $cm^{-2}$) | $E_{1/2}$ (V vs. RHE) | $E_{j=10}$ (V vs. RHE) | ΔE (V) | Ref. |
|---|---|---|---|---|---|---|
| C@$La_{0.23}Fe_{0.15}$-$Co_3O_4$/NCNTs | 0.1 M KOH | 0.15 | 0.813 | 1.604 | 0.791 | This work |
| $La_{0.23}Fe_{0.15}$-$Co_3O_4$/NCNTs | 0.1 M KOH | 0.15 | 0.806 | 1.616 | 0.810 | This work |
| CNT-$Co_3O_4$/NC | 0.1 M KOH | - | 0.840 | 1.783 | 0.943 | [6] |
| $ZnCoMnO_4$/N-rGO | 0.1 M KOH | 0.28 | 0.830 | 1.680 | 0.850 | [7] |
| Co-$Co_3O_4$@NAC | 0.1 M KOH | 0.30 | 0.795 | 1.610 | 0.815 | [8] |
| Pd@PdO–$Co_3O_4$ nanocubes | 0.1 M KOH | 0.20 | 0.727 | 1.540 | 0.813 | [9] |
| $Zn_{0.4}Ni_{0.6}Co_2O_4$/NCNTs | 0.1 M KOH | 0.21 | 0.780 | 1.642 | 0.862 | [10] |
| Co/$Co_3O_4$@ODGC | 0.1 M KOH | 0.40 | 0.800 | 1.530 | 0.730 | [11] |
| $Co_3O_4$-CuO/$Cu_2O$/C | 0.1 M KOH | 0.42 | 0.720 | 1.800 | 1.080 | [12] |
| $MnCo_2O_{4.5}$ nanocages | 0.1 M KOH | 0.28 | 0.720 | 1.640 | 0.920 | [13] |
| $NiCo_2O_4$ nanosheets | 0.1 M KOH | 0.28 | 0.740 | 1.670 | 0.930 | [14] |
| $CoFe_{1.7}Zr_{0.3}O_4$/N-rGO | 0.1 M KOH | 0.10 | 0.730 | 1.570 | 0.840 | [15] |
| $CoMn_2O_4$–$S_2$ | 0.1 M KOH | 0.32 | 0.760 | 1.580 | 0.820 | [16] |
| $La_5Ni_3Co_1O_{13-\delta}$ | 0.1 M KOH | 0.14 | 0.668 | 1.600 | 0.932 | [17] |
| $LaCo_{0.5}Ni_{0.5}O_3$ | 0.1 M KOH | 0.25 | 0.744 | 1.624 | 0.880 | [18] |
| $LaCo_{0.8}Ru_{0.2}O_{3-\delta}$ | 0.1 M KOH | 0.20 | 0.630 | 1.690 | 1.060 | [19] |
| $BaFe_{0.8}Co_{0.2}O_{3-y-\delta}(OH)_y$ | 0.1 M KOH | 0.3 | 0.675 | 1.550 | 0.875 | [20] |
| MnO/Co/PGC | 0.1 M KOH | 0.51 | 0.780 | 1.600 | 0.820 | [21] |
| Mn/Co–N–C-0.02-800 | 0.1 M KOH | 0.25 | 0.800 | 1.660 | 0.860 | [22] |
| $Co_{3-x}Mn_xO_4$/C | 0.1 M KOH | 0.18 | 0.680 | 1.780 | 1.100 | [23] |
| $Co_3O_4$/$MnO_2$-CNTs | 0.1 M KOH | 0.10 | 0.810 | 1.660 | 0.850 | [24] |
| $CuCo_2O_4$/N-CNTs | 0.1 M KOH | 0.20 | 0.798 | 1.698 | 0.900 | [25] |

## References


[1] B. Chen, Z. Jiang, J. Huang, B. Deng, L. Zhou, Z.-J. Jiang and M. Liu, *J. Mater. Chem. A,* 2018, **6**, 9517-9527.

[2] G. Chen, D. Chen, J. Huang, C. Zhang, W. Chen, T. Li, B. Huang, T. Shao, J. Li and K. K. Ostrikov, *ACS Appl. Mater. Interfaces,* 2021, **13**, 45566-45577.

[3] S. Ma, J. Huang, C. Zhang, G. Chen, W. Chen, T. Shao, T. Li, X. Zhang, T. Gong and K. K. Ostrikov, *Chem. Eng. J.,* 2022, **435**, 134859.

[4] G. Kresse and J. Furthmiiller, *Comput. Mater. Sci.,* 1996, **6**, 15-50.

[5] J. K. Nørskov, J. Rossmeisl, A. Logadottir and L. Lindqvist, *J. Phys. Chem. B,* 2004, **108**, 17886-17892.

[6] C.-C. Wang, K.-Y. Hung, T.-E. Ko, S. Hosseini and Y.-Y. Li, *J. Power Sources,* 2020, **452**, 227841.

[7] W. Liu, D. Rao, J. Bao, L. Xu, Y. Lei and H. Li, *J. Energy Chem.,* 2021, **57**, 428-435.

[8] X. Zhong, W. Yi, Y. Qu, L. Zhang, H. Bai, Y. Zhu, J. Wan, S. Chen, M. Yang, L. Huang, M. Gu, H. Pan and B. Xu, *Appl. Catal., B,* 2020, **260**, 118188.

[9] H.-C. Li, Y.-J. Zhang, X. Hu, W.-J. Liu, J.-J. Chen and H.-Q. Yu, *Adv. Energy Mater.,* 2018, **8**, 1702734.

[10] X.-T. Wang, T. Ouyang, L. Wang, J.-H. Zhong and Z.-Q. Liu, *Angew. Chem. Int. Ed.,* 2020, **59**, 6492-6499.

[11] L. Wei, J. Wang, Z. Zhao, X. Yang, S. Jiao, F. Cao, S. Tang, X. Zhang, G. Qin, Q. Liang and S. Li, *Chem. Eng. J.,* 2022, **427**, 130931.

[12] K. K. Hazarika, Y. Yamada, E. V. Matus, M. Kerzhentsev and P. Bharali, *J. Power Sources,* 2021, **490**, 229511.

[13] Z. Bai, J. Heng, Q. Zhang, L. Yang and F. Chang, *Adv. Energy Mater.,* 2018, **8**, 1802390.

[14] W. Liu, J. Bao, L. Xu, M. Guan, Z. Wang, J. Qiu, Y. Huang, J. Xia, Y. Lei and H. Li, *Appl. Surf. Sci.,* 2019, **478**, 552-559.

[15] V. Kashyap and S. Kurungot, *ACS Catal.,* 2018, **8**, 3715-3726.

[16] Z. Zhang, H. Sun, J. Li, Z. Shi, M. Fan, H. Bian, T. Wang and D. Gao, *J. Power Sources,* 2021, **491**, 229584.

[17] S. R. Choi, J.-I. Lee, H. Park, S. W. Lee, D. Y. Kim, W. Y. An, J. H. Kim, J. Kim, H.-S. Cho and J.-Y. Park, *Chem. Eng. J.,* 2021, **409**, 128226.

[18] H. Wang, W. Xu, S. Richins, K. Liaw, L. Yan, M. Zhou and H. Luo, *Electrochim. Acta,* 2019, **296**, 945-953.

[19] S. G. Chandrappa, P. Moni, D. Chen, G. Karkera, K. R. Prakasha, R. A. Caruso and A. S. Prakash, *J. Mater. Chem. A,* 2020, **8**, 20612-20620.

[20] A. I. Waidha, L. Ni, J. Ali, M. Lepple, M. Donzelli, S. Dasgupta, S. Wollstadt, L. Alff, U. I. Kramm and O. Clemens, *J. Mater. Chem. A,* 2020, **8**, 616-625.

[21] X. F. Lu, Y. Chen, S. Wang, S. Gao and X. W. D. Lou, *Adv. Mater.,* 2019, **31**, 1902339.

[22] L. Wei, L. Qiu, Y. Liu, J. Zhang, D. Yuan and L. Wang, *ACS Sustainable Chem. Eng.,* 2019, **7**, 14180-14188.

[23] C. Li, X. Han, F. Cheng, Y. Hu, C. Chen and J. Chen, *Nat. Commun.,* 2015, **6**, 7345.

[24] N. Xu, Y. Zhang, M. Wang, X. Fan, T. Zhang, L. Peng, X.-D. Zhou and J. Qiao, *Nano Energy,* 2019, **65**, 104021.

[25] H. Cheng, M.-L. Li, C.-Y. Su, N. Li and Z.-Q. Liu, *Adv. Funct. Mater.,* 2017, **27**, 1701833.